



Cite this: DOI: 10.1039/d2ee03395j

Brownian motor inspired monodirectional continuous spinning triboelectric nanogenerators for extracting energy from irregular gentle water waves†

Huijing Qiu,^{‡ac} Huamei Wang,^{‡ab} Liang Xu,^{id} *^{abc} Mingli Zheng^{ab} and Zhong Lin Wang^{*acd}

Artificial or biological Brownian motors can achieve directional motion by extracting energy from a chaotic but non-thermodynamic-equilibrium environment based on asymmetry in the potential landscape. It may inspire macroscopic mechanical energy harvesting from the environment, especially water waves, which present similar characteristics with irregular and usually small-amplitude chaotic force, imposing great challenges for conventional bulky generators that need a deterministic driving force. Here, we demonstrate a macroscopic analogue of Brownian motors for effective water wave energy harvesting based on the triboelectric nanogenerator and its networks. The design adopts a novel strategy of dual symmetry breakings to convert irregular wave excitation to internal unidirectional rotation. Meanwhile, inertia wheels are utilized to cache energy from each transient excitation for a prolonged motion. Consequently, a monodirectional continuous spinning triboelectric nanogenerator is realized for effectively extracting energy from irregular water waves, performing much superiorly to previous designs. Due to the generality of the strategies, this work points out an important paradigm for harvesting energy from random excitations on different scales in the environment by learning from microscopic molecular systems which are intrinsically adaptive to chaotic force and can have high efficiency.

Received 19th October 2022,
Accepted 22nd November 2022

DOI: 10.1039/d2ee03395j

rsc.li/ees

Broader context

Novel energy harvesting technologies can provide revolutionary foundations for fields ranging from personal devices, healthcare, Internet of Things to clean energy and carbon neutrality. A great challenge in this area is that the device should tackle with the randomness of environmental agitations as the energy source. Previous devices were designed mainly based on structures more adaptive to deterministic driving forces; thus usually an unsatisfactory performance is obtained, which greatly hinders their practical applications. Inspired by the Brownian motors at the microscopic level that can efficiently obtain energy from a chaotic environment *via* asymmetric potential landscapes, we demonstrate a monodirectional continuous spinning triboelectric nanogenerator (TENG) and its networks for effectively extracting energy from irregular gentle water waves based on the strategies of dual symmetry breakings and inertial energy caching, revealing its inherent adaptability to the randomness of chaotic environmental agitations. Unlike conventional devices that only intermittently generate pulsed output in response to low-frequency waves, the fabricated TENG can accumulate irregular wave excitations for a continuous and intermittently enhanced output, boosting the total performance. This work provides important new strategies for designing better energy harvesting devices with intrinsic adaptability to chaotic forces and random excitations of various sources in the environment.

^a Beijing Institute of Nanoenergy and Nanosystems, Chinese Academy of Sciences, Beijing, 101400, P. R. China. E-mail: xuliang@binn.cas.cn

^b School of Nanoscience and Technology, University of Chinese Academy of Sciences, Beijing, 100049, P. R. China

^c Center on Nanoenergy Research, School of Physical Science and Technology, Guangxi University, Nanning, 530004, P. R. China

^d Georgia Institute of Technology, Atlanta, Georgia, 30332-0245, USA. E-mail: zhwang@gatech.edu

† Electronic supplementary information (ESI) available. See DOI: <https://doi.org/10.1039/d2ee03395j>

‡ H. Qiu and H. Wang contributed equally to this work.

Introduction

With the threats of global warming and related climate problems,^{1–3} carbon neutrality has become an inevitable choice that relies greatly on clean energy utilization. Ocean energy, also known as blue energy, is one of the most promising clean energy sources due to its enormous global reserves, with wave energy as a typical form.^{4–6} As a traditional route for wave energy harvesting, the devices based on electromagnetic

generators still suffer from high cost and low reliability for their complex and bulky structures.⁷ Requiring a deterministic driving force, they are especially inefficient for gentle waves that are widely distributed in oceans and appear rather irregular (although a certain spectrum exists). In contrast, triboelectric nanogenerators (TENGs) open up a new technological route for blue energy harvesting, with simple unit structure and resilient distributed architecture.^{8–15}

First invented in 2012,¹⁶ the TENG is a new technology to convert mechanical energy into electricity, which is based on Maxwell's displacement current,¹⁷ and works *via* triboelectrification and electrostatic induction.^{9,13,18,19} By virtue of cost-effectiveness, easy fabrication, light weight and rich material choices,¹⁷ the TENG and its networks are regarded as a promising approach for harvesting environmental mechanical energy, exhibiting fast development.^{20–29} However, up to now, generally the designs of TENGs are still based on deterministic driving force, which is not quite adaptive to the randomness of environmental agitations.

As the microscopic level is full of thermal noise and stochastic forces, a couple of artificial and biological molecular machines can harvest energy from a chaotic environment without violating the thermodynamic laws and perform directional motion, showing intrinsic adaptability to random forces and they can achieve high efficiency.^{30–34} The structures are mainly based on the mechanism of the Brownian ratchet, which involves symmetry breaking in the potential landscape.³⁵ It is inspiring for harvesting macroscopic mechanical energy based on TENGs from the environment, especially water waves, which present similar characteristics with irregular and usually small-amplitude chaotic force, considering that present TENG designs for wave energy harvesting still suffer from the pulsed output characteristic due to irregular low-frequency wave excitations, with limited output power.

Here, inspired by the Brownian motor, a monodirectional continuous spinning triboelectric nanogenerator (CS-TENG) with a distributed network architecture is demonstrated for extracting energy from irregular gentle waves. A novel strategy of dual symmetry breakings is introduced by non-mirrored network linkers and one-way bearing enabled ratchet effect, the synergy of which allows irregular wave excitations to be rectified into internal unidirectional motions. An inertia-wheel-based energy caching strategy is further utilized to collect contributions from each transient excitation, achieving prolonged spinning. Consequently, energy from irregular gentle waves can be effectively extracted and accumulated positively each time for electricity generation without phase mismatch. Unlike conventional TENGs that only intermittently generate pulsed output in response to low-frequency waves, the fabricated CS-TENG can accumulate irregular wave excitations for a continuous and intermittently enhanced output, boosting the total performance. Due to the generality of the strategies, this work also points out an important paradigm for harvesting energy from random excitations of different scales in the environment by learning from microscopic molecular systems which are intrinsically adaptive to chaotic force and can have high efficiency.

Results and discussion

Concept, device structure and working principle

The concept of the design is shown in Fig. 1a. A TENG basically consists of a rotator fixed with inertia wheels and a stator fixed with a packaging outer shell, and is networked through upper and lower linkers. Inspired by the Brownian motors that can achieve directional motion in a chaotic environment based on asymmetry in the potential landscape,^{30–34} novel strategies of dual symmetry breakings and inertial energy caching are applied in the device, allowing continuous spinning of the rotator under irregular low-frequency excitations of water waves. First, the upper and lower linkers network the TENG at the top and bottom, respectively, forming a chiral linkage without mirror symmetry. As shown in Fig. S1, ESI,† the structure does not superimpose with its mirror image. Due to that chiral structures can introduce a torsional effect into the system under linear excitations,^{36–38} such symmetry breaking by chiral linkage can transform the random excitation of water waves into a swing motion of the outer shell by imposing a fluctuating torque on the shell. Meanwhile, a one-way bearing is adopted for mounting the shaft of the rotator, which provides a ratchet effect and only allows the rotator to have relative rotation to the shell in one direction (set as the clockwise direction in this work), similar to the Brownian ratchet. More specifically, clockwise swings of the shell can accelerate the clockwise spin of the rotator by locking them together and transmitting energy, whereas anti-clockwise swings cannot alter the rotator's motion state with free relative motion. Such symmetry breaking by ratchet effect can further convert the swing motion of the outer shell to monodirectional spinning of the rotator. Based on the dual symmetry breakings realized by rather simple structures, irregular water movement is successfully rectified to unidirectional spinning, demonstrating a motion rectification effect which refers to transforming the motion toward multiple directions to that along a single direction. Second, inertia wheels with a large moment of inertia are designed to roll with the rotator, which can enhance the power take-off from the wave due to larger input loading. The harvested mechanical energy is cached in the inertia wheel with prolonged spinning time and gradually transformed into electricity with the TENG. Owing to the unidirectionality that excludes the phase-mismatch problem, the energy from intermittent wave excitations can keep the inertia wheel accelerating, building up continuous spinning of the rotator, which is still effective even when the amplitude of the wave is small. With regard to the energy perspective, in the process, the ocean mechanical energy from waves is converted to the spin energy of the rotator, which is transformed into electric power with the relative motion of the stator and rotator in the device.

As a comparison, spring-oscillator structures and swing structures used to be applied for a prolonged response behavior after a single excitation due to their dynamic properties.^{39,40} The swing structure is shown to be able to realize an ultra-long response time, yet at the expense of low output which actually "digests" the harvested mechanical energy in a slow pace for a long duration.⁴¹ Moreover, in the systems, the phase mismatch

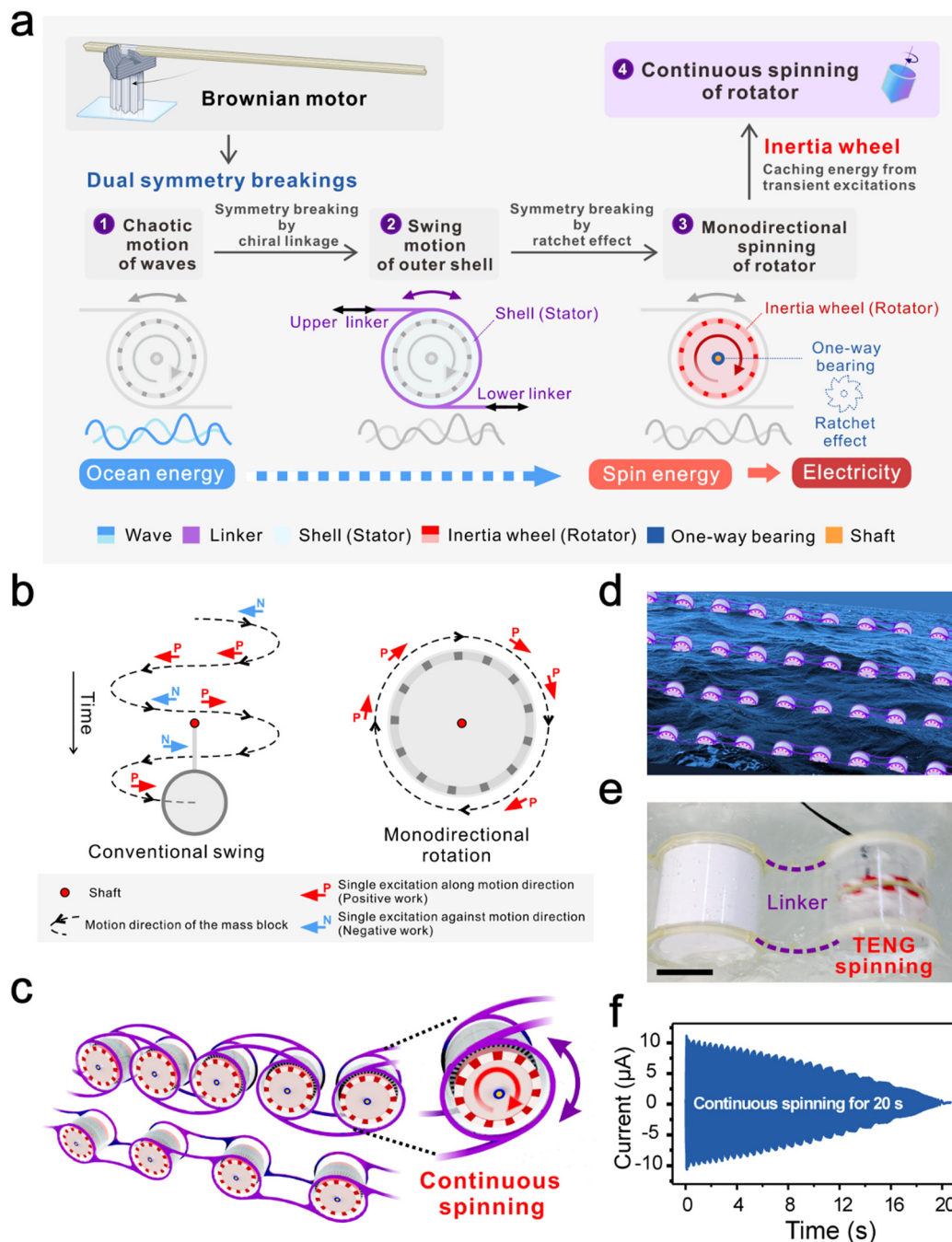


Fig. 1 Basic concept of the continuous spinning triboelectric nanogenerator (CS-TENG). (a) Schematic illustration of the general concept. Partly reproduced with permission.³³ Copyright 2022, Nature. (b) Schematic illustration of the effect of monodirectional rotation. (c) Schematic illustration of the CS-TENG chain. (d) Schematic perspective of a large-scale network of CS-TENGs for blue energy harvesting. (e) Photograph of the fabricated CS-TENG under water wave agitation. Scale bar, 10 cm. (f) Ultra-long duration of short-circuit current output after excitations.

can easily result in a negative superposing effect for sequential excitations due to the irregularity, and the systems only have high efficiency at the resonant state. Specifically, as shown in Fig. 1b, for the swing structure, although the mass block can also store the excitation energy for a prolonged swing duration, some of the excitations are against the motion direction of the mass block, contributing negative work to the system. Such phase-mismatch problem makes it difficult to accumulate

positively the contribution of each random excitation. On the contrary, the unidirectionality realized by motion rectification here ensures that each excitation is along the rotation direction of the mass block, contributing positive work to the motion; thus the energy can be fast accumulated in the rotator and inertia wheels.

The dual symmetry breakings along with energy caching substantially impart TENGs with inherent capability to work

with randomness in water waves, by the capability of converting random low-frequency excitations to persistent and cumulative monodirectional spinning that keeps on power generating. For conventional TENGs, their instant power outputs rely on the agitation intensity for the very moment, and asynchronous waves convert to electricity almost independently. Alternatively, for the CS-TENG, since the prolonged spin time of one single excitation is much more likely to overlap with the next excitation, non-simultaneous wave excitations of diverse amplitudes and frequencies can be accumulated, which accelerates the speed of the rotator to make it spin more swiftly and further elevates the power output. Thus, unlike conventional TENGs that only intermittently generate electricity in response of low-frequency wave excitations, the CS-TENG can accumulate sequential wave excitations for a continuous and intermittently-enhanced output.

The CS-TENGs are typically networked with the chiral linkage structure to form a long chain, as shown in Fig. 1c. Under the excitation of water waves, the chain will be stretched repeatedly, imposing fluctuating torque on each device *via* the chiral configuration, which effectively agitates the shell to swing. Such TENG chains can be organized with different scales for harvesting ocean

wave energy based on the demands of applications (Fig. 1d). Fig. 1e demonstrates the photograph of the fabricated device, and the wave excitations induce swift spinning of the rotator in the TENG device. Fig. 1f shows a typical output and the duration of continuous spinning transcends 20 s after excitations with high-frequency output, as shown in Fig. 1f and Movie S1 (ESI[†]).

Fig. 2a and b demonstrates the detailed structures and working process of the one-way bearing and inertia wheel. The one-way bearing is mounted between the outer shell and the shaft which is fixed with the inertia wheel. More details of the structure of the one-way bearing are shown in Fig. S2 (ESI[†]). According to the direction of the relative motion of the outer shell to the inertia wheel, the one-way bearing will switch between two working states, namely the unlock and lock states (Fig. 2b). When the shell is relatively static or rotates anti-clockwise to the inertia wheel, the bearing is unlocked, and there will be no torque transmitted through the bearing; thus the motion state of the inertia wheel will not change. Instead, when the shell rotates clockwise relative to the inertia wheel, the one-way bearing will lock the shell and the inertia wheel together, thus exerting torque to accelerate the clockwise spin

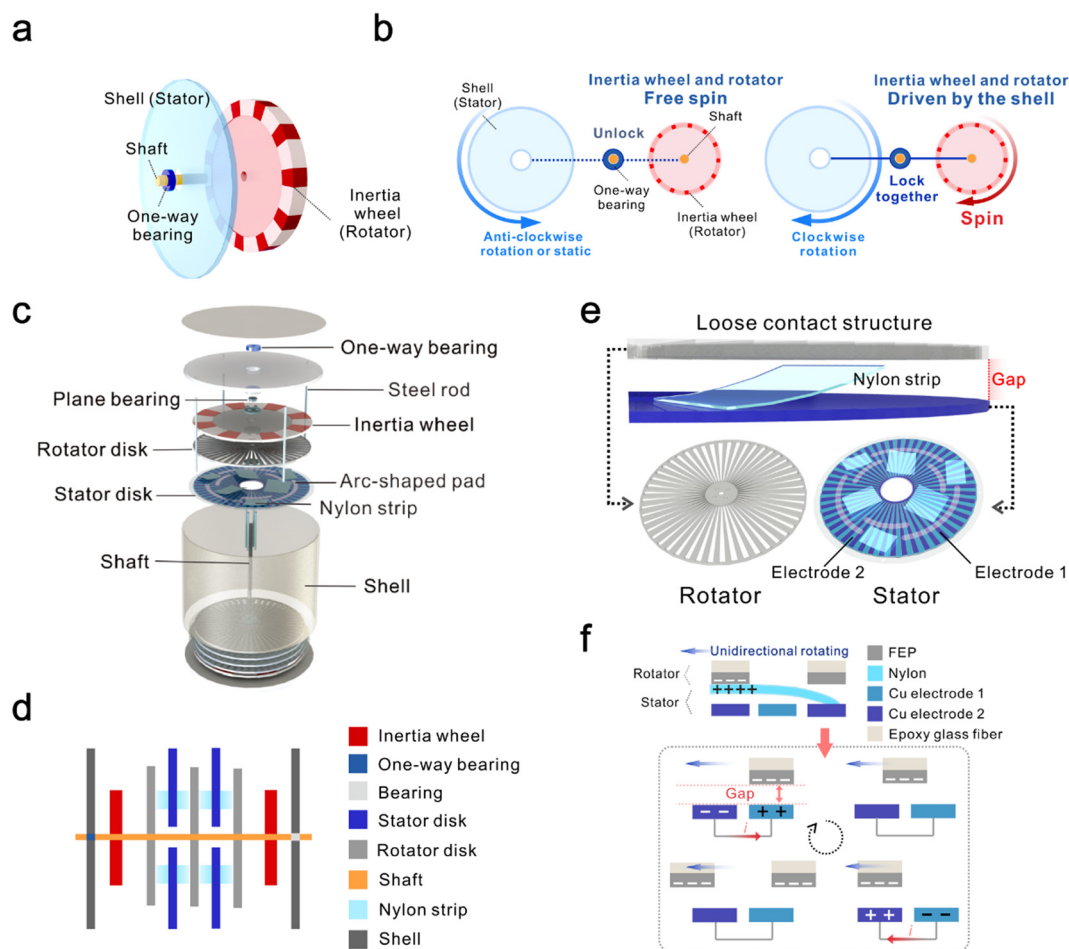


Fig. 2 Structure and working principle of the CS-TENG. (a) Schematic detailed structures of the one-way bearing and inertia wheel. (b) Working process of the one-way bearing and inertia wheel. (c) Schematic exploded view of the CS-TENG. (d) Schematic side view of the CS-TENG. (e) Schematic details of the rotator and stator disks. (f) Working principle of the TENG sub-unit.

of the inertia wheel to surpass the speed of the shell. In short, the inertia wheel is either accelerated or continues to spin clockwise, leading to a spinning state of immutable direction.

An exploded view of the whole CS-TENG device is demonstrated in Fig. 2c. The device mainly constitutes a packaging shell, the inertia wheels (typically two at the two sides to form an inertia wheel group) and TENG sub-units, which are formed by facing sides of rotator disks and stator disks. While the stator disks are assembled together with steel rods to form a total stator and fixed to the shell, the whole rotator composed of the rotator disks, the inertia wheels and the shaft is mounted inside through a group of bearings, including the one-way

bearing. In order to reduce frictional force between the rotator disk and stator disk within each TENG sub-unit, a central spacer with a proper thickness is sandwiched between adjacent rotator disks, introducing a gap between the rotator disk and stator disk, and thin arc-shaped pads are adhered on both sides of the stator disk to reduce the contact area in case of contact. Meanwhile, a loose contact structure realized by using nylon strips that fix one end to the stator disk is adopted for triboelectric charge generation.^{41–44} As a result, the total friction is considerably cut down to facilitate continuous spinning with high output. Since each stator disk or rotator disk can contribute to two sub-units with their two faces, twice as many

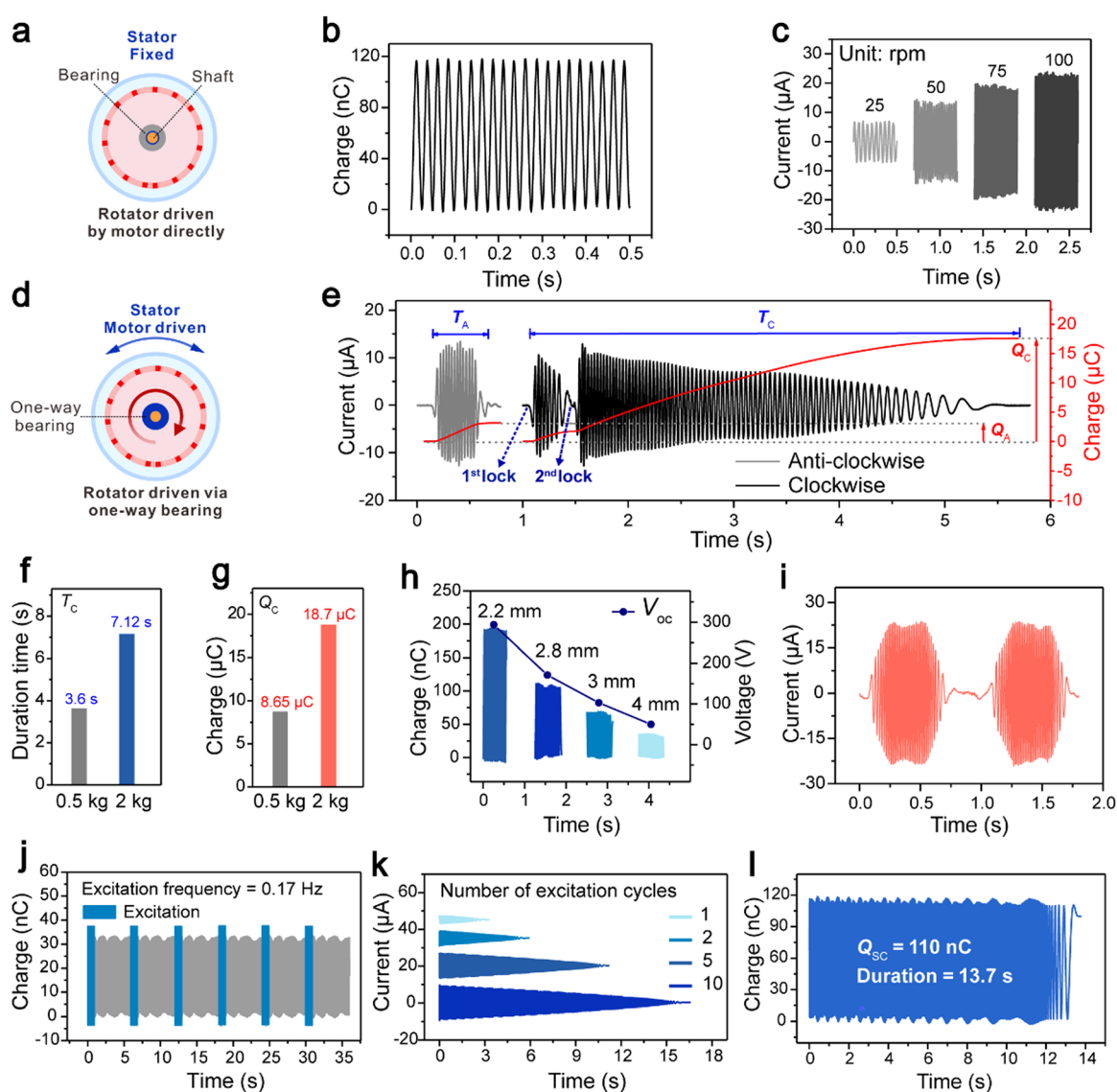


Fig. 3 Electrical characterization of the CS-TENG sub-unit in air. (a) Schematic illustration of the excitation mode with the rotator driven by a motor. (b) Transferred charges of the sub-unit under a motor speed of 50 rpm. (c) Short-circuit current of the sub-unit under different motor speeds. (d) Schematic illustration of the excitation mode with the rotator driven via the one-way bearing. (e) Typical current response of a CS-TENG sub-unit under a single clockwise or anti-clockwise excitation. (f and g) Duration time (f) and integrated charges (g) of the sub-unit under a single excitation with different inertia wheels. (h) Charges and open-circuit voltages of the sub-unit with various spacer thicknesses. (i) Short-circuit current of the sub-unit under successive excitations of 1 Hz. (j) Continuous charge output of the sub-unit under an ultra-low excitation frequency of 0.17 Hz. (k) Currents (some are shifted) and spin duration after different numbers of excitation cycles. (l) Typical output of the sub-unit after excitations with 2.8 mm spacers.

TENG sub-units can form, as shown in Fig. 2d. The number of integrated sub-units is easily expandable, and 6 rotator disks intercalated with 5 stator disks are typically adopted in this work to form 10 TENG sub-units in total.

Details of the rotator and stator disks are depicted in Fig. 2e, which adopt a radial grating structure with a periodicity of 7.5° . For the rotator disk, two fluorinated ethylene propylene (FEP) layers are adhered on both sides of an epoxy glass fiber substrate. As for the stator disk, Cu layers shaped in complementary patterned sectors are coated on both sides of an epoxy glass fiber substrate through the printed circuit board (PCB) technics, forming a pair of electrodes on both sides, namely Cu electrode 1 and 2. Apart from that, evenly-spaced nylon strips are adhered on both sides of the stator disk, whose lengths are designed to allow the free end to rub with the adjacent rotator disk for triboelectric charge generation.⁴² Owing to the periodic grating structure, low-frequency excitations can be converted to high-frequency electrical outputs. Meanwhile, the loose contact structure mitigates the intrinsic large friction in grating devices with little sacrifice of charge outputs, which notably reduces surface wear as well as enhances the robustness and durability of the device, facilitating continuous spinning.

The working mechanism of the sub-unit is shown in Fig. 2f as a conjugation of triboelectrification and electrostatic induction. The rotator disk is first charged by rotary triboelectrification with the nylon strips. Then, the relative motion between the rotator disk and the stator disk drives free electrons to move between the two electrodes on the stator due to electrostatic induction, generating alternating current.⁴⁵

Electrical characterization of the CS-TENG sub-unit in air

To examine the primary output of the CS-TENG sub-unit under well-controlled agitation conditions, two modes of excitation were applied to the device in air: in the first one the stator was fixed and the rotator was directly driven using a motor without the one-way bearing, as shown in Fig. 3a. Here, the device contains four sub-units and a central spacer of thickness 2.8 mm is typically adopted, which can produce an average gap of about 0.9 mm on each side of the stator disk that has a thickness of 1 mm. Typical short-circuit transferred charges Q_{SC} of 118 nC are obtained for a single sub-unit (Fig. 3b), and the peak-to-peak open-circuit voltage V_{OC} can achieve over 170 V (Fig. S3, ESI[†]). The short-circuit current I_{SC} increases with the rotation rate, which is around 23 μA for a rotation rate of 100 rpm, as shown in Fig. 3c. Moreover, the charge output with different rotation rates is shown in Fig. S4 ESI[†] and the output basically remains stable.

Aiming to simulate wave agitations, the second mode of excitation drives the shell (stator) instead, utilizing a pinion and rack mechanism with a conversion ratio of $2.865 \text{ deg mm}^{-1}$ (Fig. S5, ESI[†]), which triggers the spinning of the rotator disks and inertia wheels *via* the one-way bearing, as shown in Fig. 3d. A typical current response for one sub-unit in the device upon a single clockwise or anti-clockwise excitation from the stator is presented in Fig. 3e. According to the working principle of the device, the anti-clockwise rotation of the stator (relative to the rotator)

leaves the one-way bearing unlocked and the rotator's motion state unchanged (which is static here). Thus, the relative motion of the stator and rotator that decides the output only depends on the motion of the stator which is synchronous with the motor. In contrast, for relative clockwise rotation of the stator, the one-way bearing changes to the lock mode that transfers torque to accelerate the rotator to surpass the stator. Similar to a collision process, such torque transfer is instantaneous and may happen more than once, as the relative clockwise rotation of the rotator may lag behind the stator again due to energy dissipation in the rotating process. As shown in Fig. 3e, two lock events can be observed in the clockwise excitation. The output durations (T_A for the anti-clockwise case, and T_C for the clockwise case) and integrated transferred charges (Q_A for the anti-clockwise case, and Q_C for the clockwise case), which is the time integral of the absolute value of current output, are quite different (Fig. 3e). The output duration of the anti-clockwise case is the same as the excitation duration of the motor, while the duration of the clockwise case is much longer and lasts after the motor stops due to energy caching of the inertia wheel, resulting in remarkably larger output charges.

The incomparable effect of the inertia wheel on continuous spinning is well demonstrated in Fig. 3f and g, with spacer thicknesses of 4 mm and 2.8 mm, respectively. For one single clockwise excitation, integrated charges as large as 18.7 μC are transferred and the spinning lasts for 7.12 s with inertia wheels of 2 kg (the detailed curve is shown in Fig. S6, ESI[†]), which obviously outperform those of 8.65 μC and 3.6 s with a mass of 0.5 kg, as a result of a stronger inertia effect. Moreover, the output charges can be multiplied by the integrated number of the sub-unit, which only occupies a thin slice less than 2.5 mm each. Such exceptionally high charge output performance accompanied by ultralong duration time after merely one excitation marks a great advance compared with other related studies in the field.^{25,27,41} Apart from that, the dependence of outputs on the spacer thickness is investigated and presented in Fig. 3h, with associated T_C and Q_C shown in Fig. S7 (ESI[†]) and Fig. S8 (ESI[†]) respectively. As the spacer thickness increases from 2.2 mm to 4 mm, both triboelectrification and electrostatic induction attenuate, hence reducing the transferred charges from nearly 200 nC to 35 nC, with a decline in open-circuit voltage from 300 V to 50 V (peak-to-peak value).

Besides single-direction excitations, the output of the device under reciprocating excitations of 1 Hz in Fig. 3i shows a reasonably higher current exceeding 22 μA for one sub-unit, resulting from the relative motion superposition from the anti-clockwise movement of the stator and the elongated clockwise rotation of the rotator. The corresponding peak-to-peak open-circuit voltage is around 160 V (Fig. S9, ESI[†]). By virtue of the extensively lengthened rotation, literally continuous spinning that does not stop is realized even at an ultra-low drive frequency of 0.17 Hz for a device with 4 mm spacers, as presented in Fig. 3j and Movie S2 (ESI[†]), where the charge output maintains albeit transient excitations amid long intervals. More importantly, the rotation speed can also be accelerated upon more than one

excitation, boosting the spin duration to a new level. As the number of excitation cycles increases from 1 to 10, both the current value and spin duration after excitations multiply and achieve continuous spinning of about 16 s for the device with 4 mm spacers (Fig. 3k). Accordingly, for the device delivering a typical output of about 110 nC with 2.8 mm spacers, the accumulation raises the spin duration to 13.7 s (Fig. 3l), which largely transcends that of about 5 s under a single excitation.

Performance of the CS-TENG for wave energy harvesting

Based on the characterization of sub-units in different configurations, a packaged CS-TENG integrated with 10 sub-units is fabricated for wave energy harvesting, adopting a spacer thickness of 2.8 mm and inertia wheels of 1 kg, as shown in Fig. 4a. A rectification circuit presented in Fig. 4b is utilized for the total output in case of asynchrony among sub-units. For adjacent sub-units sharing the same rotator disk, the asynchrony can be neglected, and they can share one rectifier. First, the CS-TENG is characterized on the motor with well controlled excitations. A single CS-TENG sub-unit in the device yields a stable output of about 110 nC, which is nearly doubled by using two sub-units, showing good superposition capability, as presented in Fig. 4c and d. The total rectified current of 10 sub-units under a single excitation exceeds 200 μA , whose integrated transferred

charges surge to 187.25 μC and can be further enhanced with more units being integrated (Fig. 4e). The current under successive excitations as shown in Fig. 4f reasonably increases to about 300 μA . Notably, though packing 10 TENG sub-units, the device exhibits excellent sensitivity even under ultra-mild excitations. As shown in Fig. 4g, a current of about 80 μA is generated under subtle excitations of 5 mm, demonstrating its capability of harvesting energy from gentle water waves. The high output allows the device to rapid charge capacitors, as shown in Fig. 4h. With an excitation frequency of 1.75 Hz, it takes a time of 3.435 s for a 100 μF capacitor to be charged to 4 V, which varies to 6.586, 11.393, 16.07, and 32.53 s for capacitors of 0.2, 0.33, 0.47 and 1 mF, respectively, and a 2 mF capacitor can be charged to 2.96 V in 50 s. The power outputs of the device with different load resistances are also examined. The peak power can reach 14.357 mW along with an average power of 3.528 mW at a small resistance of 560 k Ω , indicating the capability of the CS-TENG to deliver superiorly high output. Considering that the total volume of the TENG sub-units is $4.16 \times 10^{-4} \text{ m}^3$, a volume peak power density of 34.50 W m^{-3} and an average power density of 8.48 W m^{-3} can be obtained. The corresponding peak currents and load voltages for each load are provided in Fig. S10 (ESI[†]).

In a water environment, as discussed above, the CS-TENG is agitated based on the chiral linkage in a network, which is

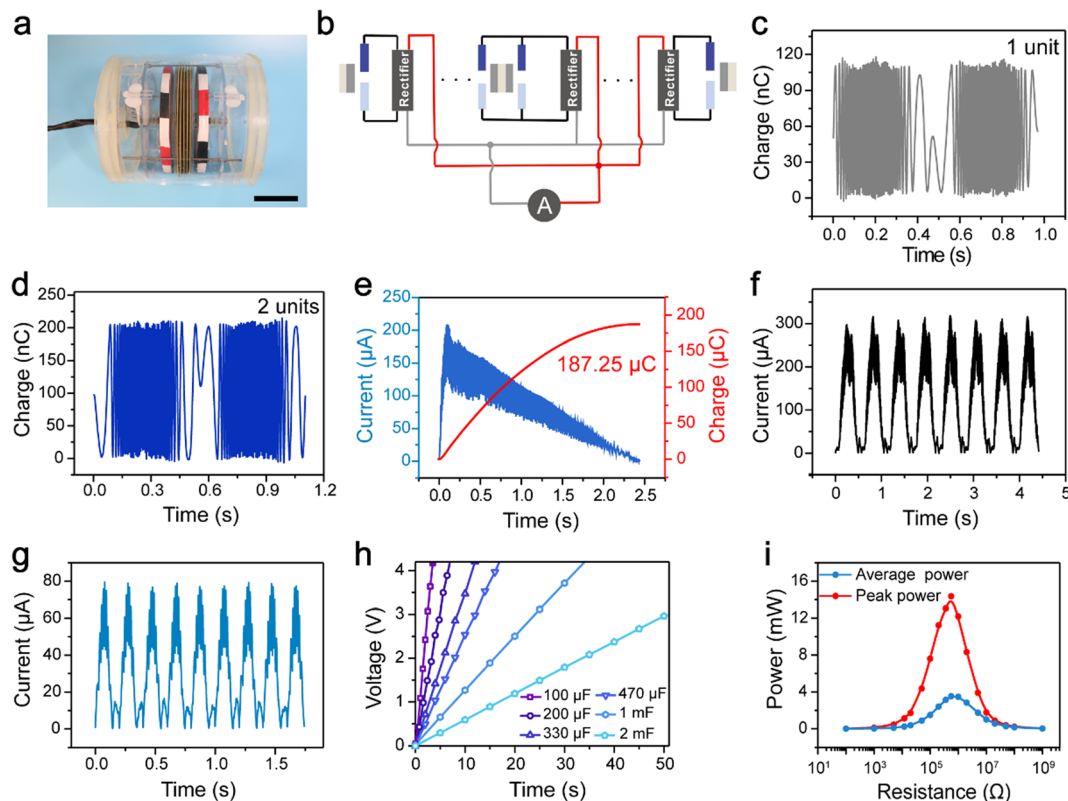


Fig. 4 Electrical characterization of the integrated CS-TENG in air. (a) Photograph of the fabricated CS-TENG. Scale bar, 5 cm. (b) Rectification circuit diagram of the CS-TENG. (c) Transferred charges of a sub-unit in the integrated device. (d) Transferred charges of two sub-units in the integrated device. (e) Rectified current and charge output of the integrated device after a single excitation. (f) Current output of the integrated device under successive excitations. (g) Current output of the integrated device under subtle excitations of 5 mm. (h) Voltages of capacitors charged by the integrated device. (i) Peak power and average power of the integrated device under various loads.

demonstrated in detail in Fig. 5a. Under wave agitations, the positions of the CS-TENGs will oscillate, and the chirally arranged linkers will bend and restore between two stressed states due to their elasticity, causing all the devices to swing back and forth, which triggers the internal rotator to spin clockwise *via* the one-way bearing. The monodirectional spin will continue after the excitation due to energy caching in the inertia wheel and will be accelerated by succeeding excitations.

A CS-TENG integrating two sub-units was tested under typical wave agitations of 0.67 Hz produced in a wave tank using wave pumps. The transferred charges of a single CS-TENG sub-unit are 115 nC, along with a peak-to-peak open-circuit voltage approaching 146 V, as shown in Fig. 5b and c. A series of photographs presented in Fig. 5d and Movie S3 (ESI[†]) directly reveal the whole process of practical devices excited by waves (because the photographing is from the back side, the rotator shows anti-clockwise rotation, which is corrected in the figure by

mirroring the photographs). The high-speed spinning can even obscure the red-and-white stripes on the wheel, as can be clearly observed. The output response of the device under water excitations from pumps on to off is captured in Fig. 5e. The current of a single CS-TENG sub-unit manifests continuity and peaks at about 24 μ A, and the output continues even after pumps are switched off owing to the afterward damping of water waves inside the tank, whose amplitude wanes gradually before vanishing. Therefore, the generated current establishes descending peak values and vanishes after about 15 s, which confirms that the CS-TENG can be effectively agitated by water waves of different amplitudes to produce outstanding outputs.

On the basis of the superior adaptability and stability of the CS-TENG for blue energy harvesting, the device is expected to be organized with different scales as a power source for supporting activities and applications in the ocean, as briefly summarized in Fig. 6a. For the CS-TENG integrated with

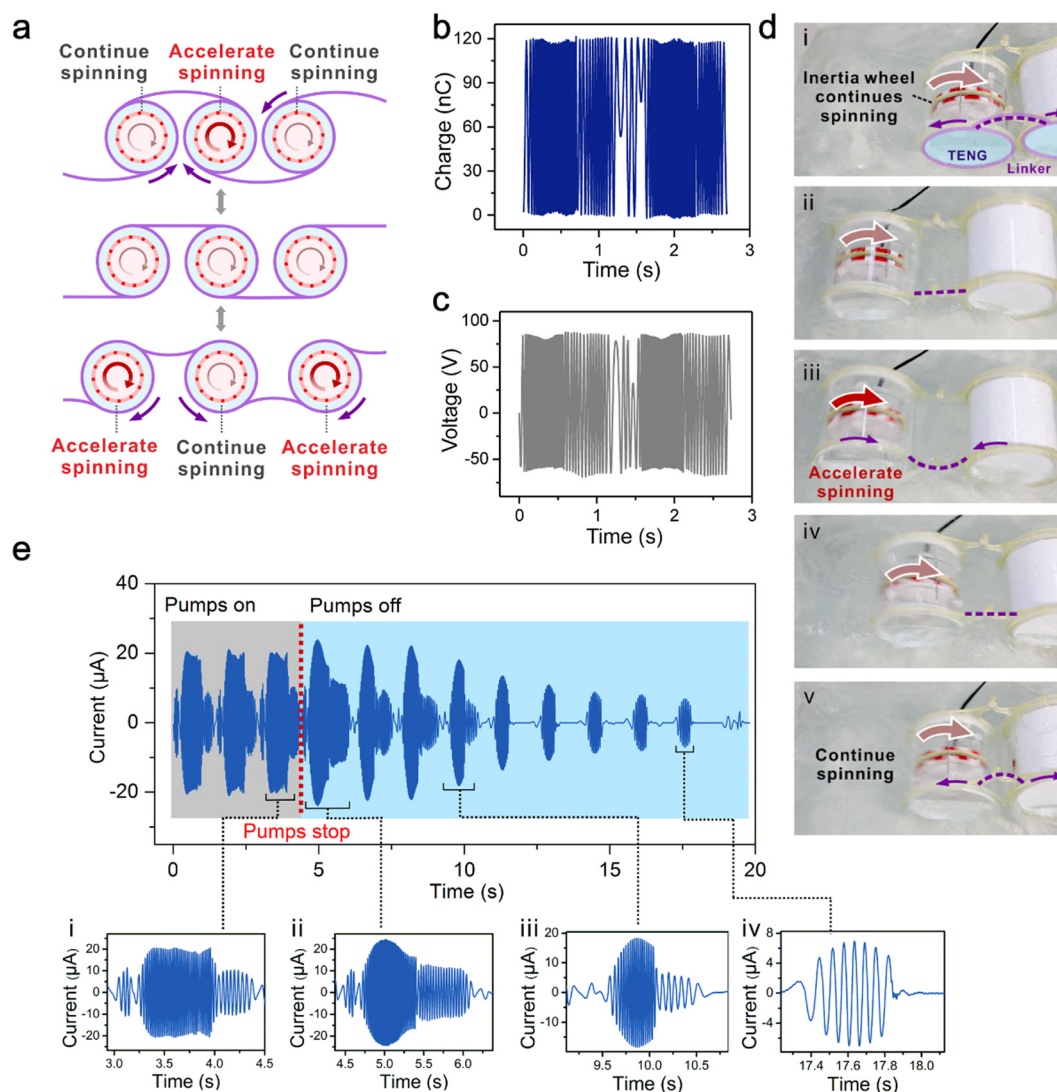


Fig. 5 Performance of the CS-TENG in water. (a) Working principle of networked devices in chiral linkage under wave excitations. (b and c) Transferred charges (b) and open-circuit voltage (c) of a sub-unit in the CS-TENG agitated by water waves. (d) Photographs (mirrored) on the working process of the device excited by waves. (e) Current output response of a sub-unit in the CS-TENG under wave excitations.

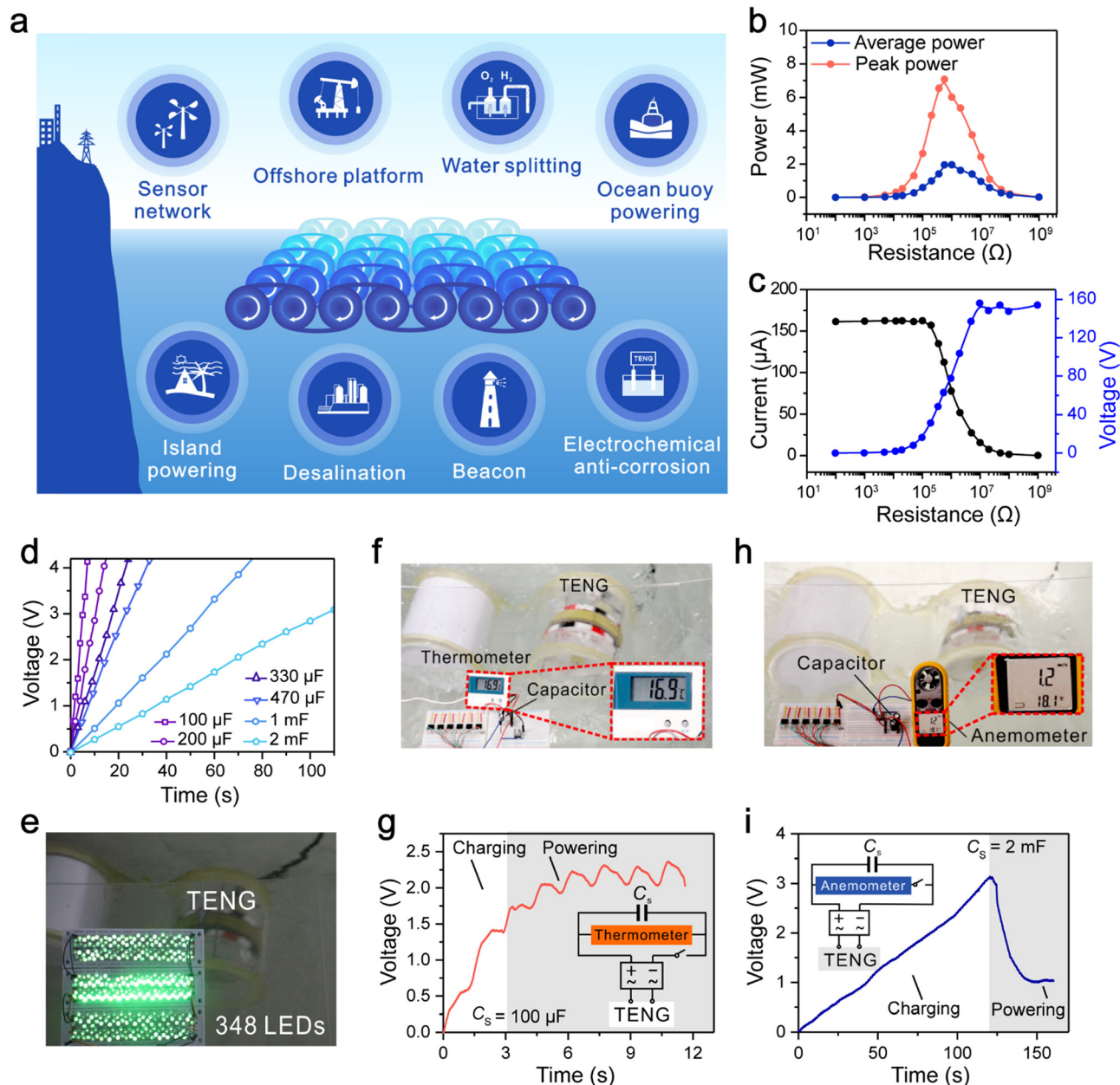


Fig. 6 Application demonstration of the CS-TENG. (a) Schematic prospect of applications based on the CS-TENG. (b) Peak power and average power of the CS-TENG with various loads in water. (c) Peak currents and load voltages of the CS-TENG with various loads in water. (d) Voltages of capacitors charged by the CS-TENG agitated by water waves. (e) Continuously powering 348 light emitting diodes (LEDs) by the CS-TENG in water. (f–i) Photographs and voltage curves of storage capacitors for the CS-TENG to power a thermometer (f and g) and an anemometer (h and i). Insets: Circuit diagram. The wave frequency is 0.67 Hz.

10 sub-units shown in Fig. 4a, the peak power and average power can reach 7.07 mW and 1.95 mW, respectively, with a small load resistance of 560 k Ω , under a low-frequency 0.67 Hz wave (Fig. 6b). Considering the total volume of the TENG sub-units, a volume peak power density of 16.99 W m⁻³ and an average power density of 4.69 W m⁻³ can be obtained. The corresponding peak currents and load voltages are shown in Fig. 6c, and a total short-circuit current curve is presented in Fig. S11 (ESI[†]), where a high value of over 175 μ A is produced in waves. The charging capability of the CS-TENG under wave agitations was also characterized. A 100 μ F capacitor can be

charged to 4 V in 6.7 s while the voltage of a 2 mF capacitor touches 3 V within 110 s, along with capacitors of 0.2, 0.33, 0.47, 1 mF being charged to 4 V in 13.7, 23.34, 31.72, and 72.86 s, respectively (Fig. 6d). In addition, it is demonstrated that the device can keep 348 light emitting diodes (LEDs) glowing almost constantly, directly verifying the successfully realized continuous spinning and power generation of the device (Fig. 6e, and Movie S4, ESI[†]).

With the confirmed exceptional performance, the power supply capability of CS-TENGs as a wave energy harvester for diverse marine self-powered systems was further exemplified in temperature sensing and wind monitoring systems as shown in

Fig. 6f–i. The temperature is acquired *via* directly connecting a 100 μF storage capacitor (C_s) with the CS-TENG and the thermometer in parallel (inset of Fig. 6g), which can be automatically started in 3 s as the capacitor voltage is charged beyond 1.5 V (Fig. 6f, g and Movie S5, ESI†) and continue working without interruption. For wind speed detection, a 2 mF capacitor is charged to 3.135 V in 120.8 s through a circuit shown in the inset of Fig. 6i; then the switch is closed to successfully power the anemometer (Fig. 6h, i, and Movie S6, ESI†) for about 25 s. The above data collectively prove the feasibility and practicability of the CS-TENG toward blue energy harvesting and self-powered marine systems.

Conclusions

In this work, inspired by the Brownian motors, a continuous spinning TENG and its networks based on novel strategies of dual symmetry breakings and inertial energy caching are demonstrated for extracting energy from irregular gentle water waves. The symmetry breaking from non-mirrored network linkers and the one-way bearing enabled ratchet effect allows the CS-TENG to convert random wave excitations into internal monodirectional rotation, and the energy caching with inertia wheels can store and accumulate discrete excitation energy for prolonged spinning. The unidirectionality excludes the phase-mismatch problem and ensures that the spinning is accelerated by new excitations at any time. Meanwhile, the inertia wheel can also increase power take-off from the wave due to larger input loading. Thus, unlike conventional TENGs that only intermittently generate electricity in response to low-frequency wave excitations, the fabricated CS-TENG can accumulate sequential wave excitations for a continuous and intermittently-enhanced output, boosting the total performance. Using radial grating sub-units assisted by the loose contact structure that reduces friction, an average power density of 4.69 W m^{-3} is delivered under water wave agitations, and self-powered systems based on the CS-TENG are demonstrated, presenting superior working capability. The research substantially imparts TENGs with inherent capability to work with randomness in water waves, and the size flexibility of TENGs allows their adaptability to different scales of wave fluctuations, demonstrating the superiority of TENGs for blue energy harvesting. Considering the generality of the strategies, this work also points out an important paradigm for harvesting energy from random excitations in the environment by learning from microscopic molecular systems which are intrinsically adaptive to chaotic force and can have high efficiency. Because the excitations can fluctuate on different scales, devices with the corresponding scale can be designed based on the symmetry breaking strategy of different detailed forms, covering the range from nanometer to meter scales.

Experimental section

Fabrication of the CS-TENG sub-unit

The substrates of both the stator and rotator disks were epoxy glass fiber sheets (1 mm in thickness). For the stator disk,

electrode layers of copper (35 μm in thickness) with complementary sectors that had the same central angle of about 3.75° were coated on both sides of the substrate with an inner diameter of 30 mm and an outer diameter of 183 mm by PCB technics. Nylon strips (25 μm in thickness) were evenly adhered on the electrode layers for triboelectric charge generation. Arc-shaped pads (about 0.6 mm in thickness) were adhered on the electrode layers for reducing the contact area. For the rotator disk, two layers of FEP films (80 μm in thickness) were adhered on two sides of the substrate with a diameter of 167 mm as triboelectric layers. Sectors corresponding to the electrode of the stator disk were cut in the FEP films with a laser cutter (PLS6.75).

Integration of the CS-TENG

The rotator disks were intercalated with acrylic central spacers (26 mm in diameter), and fixed with the inertia wheels (Cu rings with acrylic plates) using four steel rods (3 mm in diameter) and a shaft (6 mm in diameter) which went through around the center of the rotator. The stator disks were connected using four steel rods that went through around their edges. The one-way bearing (FC-6) and a normal bearing (6200ZZ) were mounted on the two ends of the shaft, which were then fixed to the shell. All the TENG sub-units and inertia wheels were encapsulated in an acrylic cylindrical shell (length: 20 cm, outer diameter: 20 cm, thickness: 5 mm). The CS-TENG was networked using polyurethane linkers which were fixed to the shell from outside.

Electrical measurements of the device

The voltage, transferred charges and current were measured using an electrometer (Keithley 6514). The data were collected mainly using a data acquisition card (NI PCI-6259) and a LabVIEW program. The device was driven by a servomotor and a linear motor (LinMot) during tests in air. Eight wave makers (RW-20) were used to generate water waves in a wave tank with a dimension of $1.32 \text{ m} \times 0.81 \text{ m}$.

Author contributions

L. X. conceived the idea. L. X., H. W., H. Q., and M. Z. designed the device and experiments. H. Q. and H. W. fabricated the device and did the experiments. H. W., L. X., and H. Q. discussed the data and prepared the figures. L. X., H. W., H. Q., and Z. L. W. wrote and revised the manuscript. L. X. and Z. L. W. guided the project.

Conflicts of interest

The authors declare no conflict of interest.

Acknowledgements

The research was supported by the National Key R & D Project from the Ministry of Science and Technology (no. 2021YFA1201603 and 2021YFA1201601), the National Natural Science Foundation of China (no. 51605033 and 51735001), and the Youth Innovation Promotion Association, CAS (no. 2019170).

References

- 1 A. Timmermann, J. Oberhuber, A. Bacher, M. Esch, M. Latif and E. Roeckner, *Nature*, 1999, **398**, 694–697.
- 2 V. Barbarossa, J. Bosmans, N. Wanders, H. King, M. F. P. Bierkens, M. A. J. Huijbregts and A. M. Schipper, *Nat. Commun.*, 2021, **12**, 1701.
- 3 M. Yamaguchi, J. C. L. Chan, I.-J. Moon, K. Yoshida and R. Mizuta, *Nat. Commun.*, 2020, **11**, 47.
- 4 S. H. Salter, *Nature*, 1974, **249**, 720–724.
- 5 J. D. Isaacs and W. R. Schmitt, *Science*, 1980, **207**, 265.
- 6 O. Ellabban, H. Abu-Rub and F. Blaabjerg, *Renewable Sustainable Energy Rev.*, 2014, **39**, 748–764.
- 7 J. Tollefson, *Nature*, 2014, **508**, 302–304.
- 8 Z. L. Wang, *Nature*, 2017, **542**, 159–160.
- 9 C. S. Wu, A. C. Wang, W. B. Ding, H. Y. Guo and Z. L. Wang, *Adv. Energy Mater.*, 2019, **9**, 1802906.
- 10 X. Yang, L. Xu, P. Lin, W. Zhong, Y. Bai, J. Luo, J. Chen and Z. L. Wang, *Nano Energy*, 2019, **60**, 404–412.
- 11 L. Xu, T. Jiang, P. Lin, J. J. Shao, C. He, W. Zhong, X. Y. Chen and Z. L. Wang, *ACS Nano*, 2018, **12**, 1849–1858.
- 12 H. Wang, L. Xu and Z. Wang, *Nanoenergy Adv.*, 2021, **1**, 32–57.
- 13 Z. L. Wang, *Faraday Discuss.*, 2014, **176**, 447–458.
- 14 N. N. Zhai, Z. Wen, X. P. Chen, A. M. Wei, M. Sha, J. J. Fu, Y. N. Liu, J. Zhong and X. H. Sun, *Adv. Energy Mater.*, 2020, **10**, 2001041.
- 15 X. L. Wei, Z. Wen, Y. N. Liu, N. N. Zhai, A. M. Wei, K. Feng, G. T. Yuan, J. Zhong, Y. H. Qiang and X. H. Sun, *Nano-Micro Lett.*, 2020, **12**, 1–10.
- 16 F. R. Fan, Z. Q. Tian and Z. Lin Wang, *Nano Energy*, 2012, **1**, 328–334.
- 17 Z. L. Wang, *Mater. Today*, 2017, **20**, 74–82.
- 18 Z. L. Wang, J. Chen and L. Lin, *Energy Environ. Sci.*, 2015, **8**, 2250–2282.
- 19 S. Niu and Z. L. Wang, *Nano Energy*, 2015, **14**, 161–192.
- 20 J. Wang, S. Li, F. Yi, Y. Zi, J. Lin, X. Wang, Y. Xu and Z. L. Wang, *Nat. Commun.*, 2016, **7**, 12744.
- 21 J. Bae, J. Lee, S. Kim, J. Ha, B.-S. Lee, Y. Park, C. Choong, J.-B. Kim, Z. L. Wang, H.-Y. Kim, J.-J. Park and U. I. Chung, *Nat. Commun.*, 2014, **5**, 4929.
- 22 J. Xiong, P. Cui, X. Chen, J. Wang, K. Parida, M.-F. Lin and P. S. Lee, *Nat. Commun.*, 2018, **9**, 4280.
- 23 G. Yao, L. Xu, X. Cheng, Y. Li, X. Huang, W. Guo, S. Liu, Z. L. Wang and H. Wu, *Adv. Funct. Mater.*, 2020, **30**, 1907312.
- 24 H. Qin, L. Xu, S. Lin, F. Zhan, K. Dong, K. Han, H. Wang, Y. Feng and Z. L. Wang, *Adv. Funct. Mater.*, 2022, **32**, 2111662.
- 25 L. Liu, X. Yang, L. Zhao, H. Hong, H. Cui, J. Duan, Q. Yang and Q. Tang, *ACS Nano*, 2021, **15**, 9412–9421.
- 26 H. Wang, L. Xu, Y. Bai and Z. L. Wang, *Nat. Commun.*, 2020, **11**, 4203.
- 27 C. Zhang, L. He, L. Zhou, O. Yang, W. Yuan, X. Wei, Y. Liu, L. Lu, J. Wang and Z. L. Wang, *Joule*, 2021, **5**, 1613–1623.
- 28 X. K. Xie, X. P. Chen, C. Zhao, Y. N. Liu, X. H. Sun, C. Z. Zhao and Z. Wen, *Nano Energy*, 2021, **79**, 105439.
- 29 L. J. Xie, N. N. Zhai, Y. N. Liu, Z. Wen and X. H. Sun, *Research*, 2021, **2021**, 9143762.
- 30 R. D. Astumian, *Science*, 1997, **276**, 917–922.
- 31 W. Junge, H. Sielaff and S. Engelbrecht, *Nature*, 2009, **459**, 364–370.
- 32 A.-K. Pumm, W. Engelen, E. Kopperger, J. Isensee, M. Vogt, V. Kozina, M. Kube, M. N. Honemann, E. Bertolin, M. Langecker, R. Golestanian, F. C. Simmel and H. Dietz, *Nature*, 2022, **607**, 492–498.
- 33 H. Hess, *Nature*, 2022, **607**, 456–457.
- 34 H. Ramezani and H. Dietz, *Nat. Rev. Genet.*, 2020, **21**, 5–26.
- 35 R. D. Astumian, *Phys. Chem. Chem. Phys.*, 2007, **9**, 5067–5083.
- 36 T. Frenzel, M. Kadic and M. Wegener, *Science*, 2017, **358**, 1072–1074.
- 37 B. Jenett, C. Cameron, F. Tourlomousis, A. P. Rubio, M. Ochalek and N. Gershenfeld, *Sci. Adv.*, 2020, **6**, eabc9943.
- 38 X. L. Yu, J. Zhou, H. Y. Liang, Z. Y. Jiang and L. L. Wu, *Prog. Mater. Sci.*, 2018, **94**, 114–173.
- 39 L. Xu, Y. Pang, C. Zhang, T. Jiang, X. Chen, J. Luo, W. Tang, X. Cao and Z. L. Wang, *Nano Energy*, 2017, **31**, 351–358.
- 40 Y. Bai, L. Xu, C. He, L. Zhu, X. Yang, T. Jiang, J. Nie, W. Zhong and Z. L. Wang, *Nano Energy*, 2019, **66**, 104117.
- 41 Z. Lin, B. Zhang, H. Guo, Z. Wu, H. Zou, J. Yang and Z. L. Wang, *Nano Energy*, 2019, **64**, 103908.
- 42 J. Chen, X. Wei, B. Wang, R. Li, Y. Sun, Y. Peng, Z. Wu, P. Wang and Z. L. Wang, *Adv. Energy Mater.*, 2021, **11**, 2102106.
- 43 P. H. Wang, L. Pan, J. Y. Wang, M. Y. Xu, G. Z. Dai, H. Y. Zou, K. Dong and Z. L. Wang, *ACS Nano*, 2018, **12**, 9433–9440.
- 44 J. Cheng, W. B. Ding, Y. L. Zi, Y. J. Lu, L. H. Ji, F. Liu, C. S. Wu and Z. L. Wang, *Nat. Commun.*, 2018, **9**, 1–11.
- 45 S. Niu, Y. Liu, X. Chen, S. Wang, Y. S. Zhou, L. Lin, Y. Xie and Z. L. Wang, *Nano Energy*, 2015, **12**, 760–774.